



Pb-isotopic evidence for an early, enriched crust on Mars



J.J. Bellucci ^{a,*}, A.A. Nemchin ^{a,b}, M.J. Whitehouse ^a, M. Humayun ^c, R. Hewins ^{d,e}, B. Zanda ^d

^a Department of Geosciences, Swedish Museum of Natural History, SE-104 05 Stockholm, Sweden

^b Department of Applied Geology, Curtin University, Perth, WA 6845, Australia

^c Department of Earth, Ocean and Atmospheric Science and National High Magnetic Field Laboratory, Florida State University, Tallahassee, FL 32310, USA

^d Institut de Minéralogie, de Physique des Matériaux, et de Cosmochimie (IMPMC) – Sorbonne Université – Muséum National d'Histoire Naturelle, UPMC Université Paris 06, UMR CNRS 7590, IRD UMR 206, 75005 Paris, France

^e Department of Earth and Planetary Sciences, Rutgers University, Piscataway, NJ 08854, USA

ARTICLE INFO

Article history:

Received 12 August 2014

Received in revised form 12 November 2014

Accepted 17 November 2014

Available online 2 December 2014

Editor: A. Yin

Keywords:

Mars

Martian geochemistry

Pb isotopes

Martian crust

NWA 7533

Black Beauty

ABSTRACT

Martian meteorite NWA 7533 is a regolith breccia that compositionally resembles the Martian surface measured by orbiters and landers. NWA 7533 contains monzonitic clasts that have zircon with U-Pb ages of 4.428 Ga. The Pb isotopic compositions of plagioclase and alkali feldspars, as well as U-Pb isotopic compositions of chlorapatite in the monzonitic clasts of NWA 7533 have been measured by Secondary Ion Mass Spectrometry (SIMS). The U-Pb isotopic compositions measured from the chlorapatite in NWA 7533 yield an age of 1.357 ± 81 Ga (2σ). The least radiogenic Pb isotopic compositions measured in plagioclase and K-feldspar lie within error of the 4.428 Ga Geochron. These data indicate that the monzonitic clasts in NWA 7533 are a product of a differentiation history that includes residence in a reservoir that formed prior to 4.428 Ga with a μ -value ($^{238}\text{U}/^{204}\text{Pb}$) of at least 13.4 ± 1.7 (2σ) and a κ -value ($^{232}\text{Th}/^{238}\text{U}$) of ~ 4.3 . This μ -value is more than three times higher than any other documented Martian reservoir. These results indicate either the Martian mantle is significantly more heterogeneous than previously thought (μ -value of 1–14 vs. 1–5) and/or the monzonitic clasts formed by the melting of Martian crust with a μ -value of at least 13.4. Therefore, NWA 7533 may contain the first isotopic evidence for an enriched, differentiated crust on Mars.

© 2014 The Authors. Published by Elsevier B.V. This is an open access article under the CC BY-NC-ND license (<http://creativecommons.org/licenses/by-nc-nd/3.0/>).

1. Introduction

Currently, all of the constraints placed on the chemical and isotopic differentiation of Mars have come from studies of the shergottite, nakhelite, and chassignite (SNC) meteorites (e.g., Borg et al., 2005; Bouvier et al., 2005, 2008, 2009; Chen and Wasserburg, 1986; Debaile et al., 2007; Gaffney et al., 2007; Lee and Halliday, 1995; Nakamura et al., 1982). The SNC meteorite group comprises mafic and ultramafic rocks with a relatively limited compositional and age range (0.16–1.3 Ga, e.g., Nyquist et al., 2001 and references therein). Chemical and isotopic investigations of SNCs have yielded invaluable information about the timing and formation of the Martian core and mantle geochemical reservoirs (e.g., Debaile et al., 2007; Foley et al., 2005, and Lee and Halliday, 1995). The U-Th-Pb history of the Martian mantle has been constrained using the Pb isotopic system, which indicates that the Martian mantle has a relatively limited range in μ -values ($^{238}\text{U}/^{204}\text{Pb}$) of 1–5 and a bulk silicate μ defined as ~ 3 (Borg et al., 2005; Bou-

vier et al., 2008, 2009; Chen and Wasserburg, 1986; Gaffney et al., 2007, and Nakamura et al., 1982). These values are significantly lower than the Earth and the Moon, which have μ -values of 8–10 and 100–200 respectively (e.g., Asmerom and Jacobsen, 1993; Nemchin et al., 2011, and Zartman and Haines, 1988).

The chemical composition of the SNCs does not closely match the measured composition of the Martian surface determined by the Odyssey Orbiter, Viking Lander, Pathfinder Lander, or Mars Exploration Rovers (Boynton et al., 2007; Clark et al., 1982; Foley et al., 2003; Gellert et al., 2006, and McSween et al., 2009). In contrast, the newly described Martian regolith breccia NWA 7533 may be a more typical example of the Martian crust (Agee et al., 2013 and Humayun et al., 2013). NWA 7533 has a fine-grained matrix of alkali basaltic composition resembling the composition of the rocks and soils from Gusev crater and contains evolved monzonitic clasts, clast-laden impact melt rock, melt spherules, and microbasaltic melt rock. The monzonitic clasts contain an evolved mineral assemblage comprising alkali feldspar, plagioclase, chlorapatite, ilmenite, several types of pyroxene, and trace zircon. The clasts contain elevated concentrations of highly siderophile elements (for their MgO content) and alkali feldspars and pyroxenes have exsolved textures, which is consistent with monzonite

* Corresponding author.

E-mail address: jeremy.bellucci@gmail.com (J.J. Bellucci).

formation by differentiation of large impact melt sheets (Humayun et al., 2013). Even coarser grained, igneous textures are present in large impact melt sheets on Earth (e.g., Sudbury, Grieve et al., 1991). Therefore, the monzonite was likely formed by impact melting of Martian protocrust.

Some zircon grains preserved in the monzonitic clasts have concordant U–Pb ages of 4.428 ± 28 Ga while others fall on a discordia line between 4.428 ± 28 and 1.712 ± 85 Ga (all errors 2σ , Humayun et al., 2013). Therefore, the protocrust from which the monzonite was derived must have been extracted from the Martian mantle before 4.428 Ga. Since the monzonitic clasts have abundant plagioclase, K-feldspar, and chlorapatite, a well-constrained thermal history can be constructed and the Pb isotopic composition of the feldspars can be used to model the U–Th–Pb evolution of the monzonite (cf. Gancarz and Wasserburg, 1977; Ludwig and Silver, 1977; Kamber et al., 2003, and Oversby, 1978). Apatite has a closure temperature of ~ 450 – 500 °C (Cherniak et al., 1991 and Chamberlain and Bowring, 2001) and should constrain the age of the last thermal event experienced by the evolved clasts in NWA 7533, as demonstrated for lunar breccias (e.g., Grange et al., 2009 and Nemchin et al., 2009). Feldspars contain little to no U but relatively abundant Pb, and therefore retain their Pb isotopic composition from the time of the last equilibration event. As such, the independent chronology of the rock and the Pb isotopic composition of feldspars can be used to define the μ - and κ -values in the reservoir (s) from which the monzonitic clasts were derived.

2. Analytical methods

The U–Pb apatite analyses were performed using a CAMECA IMS1280 large geometry SIMS instrument at the Swedish Museum of Natural History, Stockholm (NordSIM facility). Prior to SIMS analysis, the sample was cleaned in an ultrasonic bath with distilled water and ethanol, dried and then coated with gold. A -13 kV molecular oxygen beam (O_2^-) was imaged through a 150 μm aperture, giving a current of ~ 4 nA in an elliptical, ~ 15 μm spot. Secondary ions were extracted from the sample at $+10$ kV and admitted, via high magnification ($160\times$) transfer optics, to the mass spectrometer operating at a mass resolution ($M/\Delta M$) of 5400. In order to minimize possible surface contamination (most likely from sample polishing and gold coating) each analysis was pre-sputtered for 80 s using a 25×25 μm raster. This was followed by a series of automated centering and optimization procedures using the matrix Ca_2PO_4 peak (mass 175), namely: secondary beam alignment in the 4000 μm field aperture (field of view on the sample of 25 μm), mass calibration adjustment and optimization of secondary ion energy in the 45 eV energy window. The peak-hopping data collection routine consisted of 32 cycles through the mass stations, with signals measured on a low-noise ion counting electron multiplier with a 44 ns electronically gated dead time.

U/Pb ratios in the phosphates have been calibrated using a piece of an apatite crystal (BRA) with an age of 2058 Ma and U concentration of 67 ppm as characterized by ID-TIMS (Nemchin et al., 2009). Data for this reference apatite fall on a slope of ~ 1.8 in the $\log(206Pb/238U)$ vs. $\log(238U^{16}O/238U)$ coordinate space. This slope was used for the calibration of U–Pb ratios in the Martian apatites following a similar protocol to that utilized for the calibration of U–Pb ratios from ion probe zircon analyses in this laboratory (e.g. Whitehouse et al., 1999).

The Pb isotopic compositions of plagioclase and alkali-feldspar were determined using the same instrument used for the apatite geochronology, closely following the experimental protocol of Whitehouse et al. (2005) and Rose-Koga et al. (2012). An area of 25×25 μm was rastered for 70 s prior to Pb isotopic analysis to minimize surface contamination. A 200 μm aperture was used re-

sulting in a 9 nA O_2^- primary beam and 20 μm circular spot on the surface of the sample. The mass resolution of the mass spectrometer during Pb isotopic analyses was 4860 ($M/\Delta M$). Analyses were conducted in multi-collector mode using an NMR field sensor to control the stability of the magnetic field. Lead isotopic ratios were measured in low noise ion-counting electron multipliers for 160 cycles with a count time of 10 s, resulting in a total collection time of 1600 s. Mass fractionation and gain calibrations between detectors were performed by bracketing the unknowns with analyses of USGS basaltic glass reference material BCR-2G (~ 11 $\mu g/g$ Pb). Corrections to the unknown measurements were performed using values from Woodhead and Hergt (2000) and a linear gain calibration. External reproducibility in $^{208}Pb/^{206}Pb$, $^{207}Pb/^{204}Pb$, and $^{206}Pb/^{204}Pb$ of BCR-2G was 0.2% , 0.2% , and 0.6% , respectively (95% confidence limits on the weighted mean). Subsequent to Pb isotopic analyses, the $^{238}U/^{208}Pb$ was measured on each analytical spot by peak jumping between masses ^{208}Pb and ^{238}U . Ions were collected in the central electron multiplier and raw U/Pb ratios were converted to elemental ratios using the relative sensitivity factors determined by measuring BCR-2G and the natural isotopic abundances of Pb and U.

3. Results

The locations of U–Pb in phosphate analyses and isotopic ratios are shown in Fig. 1 and presented in Table 1. Because a large group of the phosphates had very low measured $^{206}Pb/^{204}Pb$ ratios, specifically <20 , a 3-D model was used to calculate ages (e.g., Levchenkov and Shukolyukov, 1970; Ludwig, 2012). In this approach, each individual data point in 3-dimensional space ($^{207}Pb/^{206}Pb$ vs. $^{238}U/^{206}Pb$ vs. $^{204}Pb/^{206}Pb$) is projected onto a traditional 2-dimensional Tera-Wasserburg Concordia diagram ($^{207}Pb/^{206}Pb$ vs. $^{238}U/^{206}Pb$), obviating the requirement to know the composition of initial Pb. The U–Pb age obtained from the NWA 7533 chlorapatites is 1.357 ± 81 Ga (2σ , Fig. 2) and is in good agreement with the 1.345 ± 45 Ga U–Pb age of phosphates reported from the paired meteorite NWA 7034 (Yin et al., 2014).

The specific mineralogy of each clast and feldspar, as well as the locations of all spot analyses of the Pb-isotope analytical data are shown in Fig. 3 and Table 2. The Pb isotopic compositions of plagioclase and alkali-feldspar crystals in monzonitic clasts of NWA 7533 display a linear trend with a roughly bi-modal distribution (Fig. 4). Some of the plagioclase analyses (33%) are extremely un-radiogenic in $^{207}Pb/^{204}Pb$ and $^{206}Pb/^{204}Pb$, plotting within error of the 4.428 Ga Geochron (Holmes, 1946 and Houtermans, 1946, Fig. 4). The 4.428 Geochron is defined as a line representing single-stage Pb growth in a reservoir with any μ -value from primordial Pb (Canyon Diablo Troilite, Chen and Wasserburg, 1983) at 4.567 Ga to 4.428 Ga. All of the analyzed alkali feldspar and some of the plagioclase (66%) have significantly more radiogenic compositions (Fig. 4). Additionally, a matrix-bound plagioclase grain (Clast 3) has a similar un-radiogenic Pb isotopic composition to clast-bound plagioclase, while matrix-bound anti-perthite and perthite grains (Clasts 4 and 6) overlap in composition with clast-bound K-feldspar. The radiogenic population of feldspar plots within error of the least radiogenic phosphate (Tables 1 and 2, Supplementary Fig. 1). All of the measured compositions lie above the field defined by the leached residues of whole rock and mineral separates from the SNC meteorites in the $^{207}Pb/^{204}Pb$ vs. $^{206}Pb/^{204}Pb$ diagram (green field, Fig. 4, Borg et al., 2005; Bouvier et al., 2005, 2008, 2009; Gaffney et al., 2007).

4. Discussion

The enrichment in $^{207}Pb/^{204}Pb$ measured in the monzonitic feldspars relative to the SNC meteorites is indicative of an early

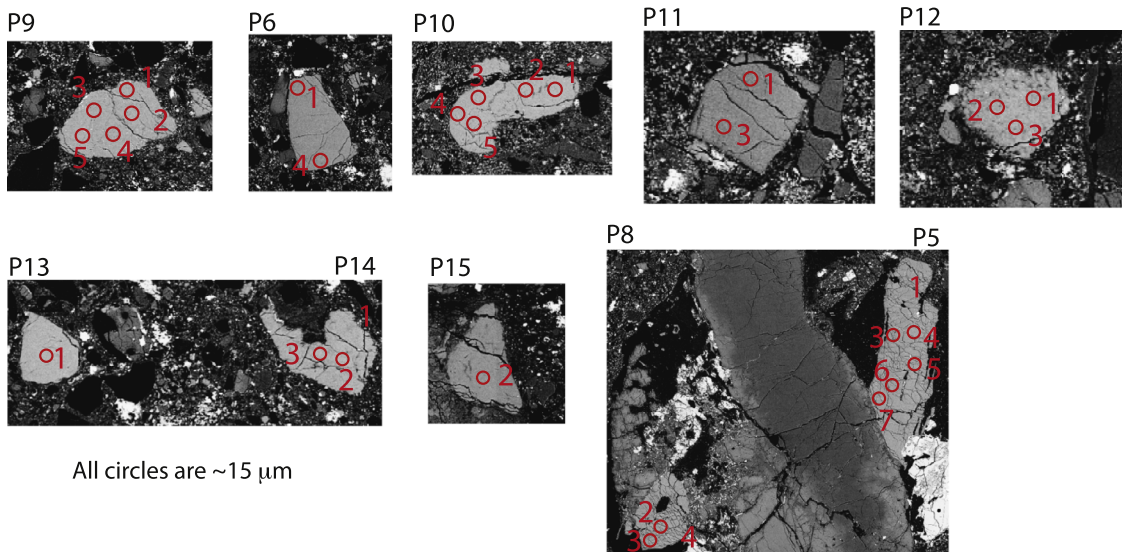


Fig. 1. Backscatter electron images and locations of spot analyses of phosphates of NWA 7533. All circles are $\sim 15 \mu\text{m}$ in diameter.

Table 1
Pb and U isotopic compositions of phosphates.

	$\frac{^{238}\text{U}}{^{206}\text{Pb}}$	σ (%)	$\frac{^{207}\text{Pb}}{^{206}\text{Pb}}$	σ (%)	$\frac{^{204}\text{Pb}}{^{206}\text{Pb}}$	σ (%)	U ($\mu\text{g/g}$)	$\frac{^{208}\text{Pb}}{^{204}\text{Pb}}$	2σ	$\frac{^{207}\text{Pb}}{^{204}\text{Pb}}$	2σ	$\frac{^{206}\text{Pb}}{^{204}\text{Pb}}$	2σ	$\frac{^{207}\text{Pb}}{^{206}\text{Pb}}$	2σ	$\frac{^{208}\text{Pb}}{^{206}\text{Pb}}$	2σ
p10@1	0.53	3.33	0.91	5.20	0.06	11.29	1.5	45.6	10.1	15.1	3.4	16.6	3.7	0.911	0.089	2.75	0.27
p10@2	0.09	4.06	0.99	1.88	0.06	4.27	0.7	37.9	3.2	15.8	1.3	16.1	1.4	0.981	0.036	2.35	0.09
p10@3	0.42	4.73	0.92	3.71	0.06	8.91	0.8	40.6	7.2	16.5	2.9	18.1	3.2	0.911	0.067	2.24	0.17
p10@4	1.39	1.56	0.66	2.92	0.05	7.08	5.2	34.5	4.9	14.3	2.0	21.6	3.1	0.665	0.039	1.60	0.10
p10@5	1.14	2.05	0.72	4.07	0.04	10.42	4.8	40.0	8.4	16.7	3.5	23.2	4.8	0.718	0.058	1.72	0.15
p11@1	2.06	1.47	0.58	3.12	0.04	7.92	12.2	46.1	7.3	14.9	2.4	25.6	4.1	0.582	0.036	1.80	0.11
p11@3	1.74	1.82	0.60	2.59	0.04	6.76	4.8	48.2	6.5	15.9	2.2	27.0	3.7	0.589	0.031	1.79	0.09
p12@1	0.11	5.24	0.95	2.55	0.06	5.73	1.4	36.8	4.2	15.3	1.7	16.2	1.9	0.942	0.047	2.27	0.12
p12@2	0.06	5.97	0.97	2.27	0.07	5.14	0.5	35.4	3.6	15.0	1.5	15.3	1.6	0.980	0.044	2.32	0.11
p12@3	0.05	4.35	0.98	1.79	0.07	3.95	0.3	35.1	2.7	14.0	1.1	14.5	1.1	0.966	0.035	2.42	0.09
p13@1	0.30	3.70	0.93	3.39	0.07	7.42	1.7	33.6	4.9	13.4	2.0	14.4	2.1	0.932	0.063	2.33	0.16
p14@1	0.99	1.94	0.73	3.89	0.05	9.21	6.9	47.8	8.7	14.1	2.6	19.5	3.6	0.723	0.056	2.45	0.19
p14@2	0.32	3.48	0.86	3.24	0.06	7.17	5.8	48.9	6.9	13.1	1.9	15.4	2.2	0.847	0.055	3.16	0.20
p14@3	0.33	4.10	0.86	2.86	0.06	6.62	6.0	52.1	6.8	14.5	1.9	17.1	2.3	0.849	0.049	3.05	0.17
p15@2	1.83	1.49	0.59	2.85	0.04	7.03	83.0	53.3	7.5	14.0	2.0	24.0	3.4	0.586	0.033	2.22	0.12
p6@1	0.68	3.07	0.83	4.80	0.06	10.43	5.7	32.3	6.7	13.8	2.8	16.6	3.5	0.828	0.076	1.94	0.19
p6@4	0.77	3.27	0.92	4.43	0.06	10.45	3.4	35.1	7.3	15.6	3.2	17.5	3.7	0.890	0.079	2.00	0.19
p9@1	0.34	3.87	1.00	3.21	0.07	6.87	0.8	31.9	4.4	13.6	1.8	14.1	1.9	0.962	0.061	2.26	0.15
p9@2	0.37	3.49	0.84	3.22	0.06	7.16	1.0	33.5	4.8	13.3	1.9	15.6	2.2	0.853	0.055	2.15	0.14
p9@3	0.30	3.52	0.89	2.83	0.06	6.33	0.4	37.6	4.7	15.1	1.9	17.3	2.2	0.874	0.047	2.17	0.12
p9@4	0.31	3.33	0.89	2.87	0.06	6.80	0.6	38.2	5.2	15.6	2.1	17.7	2.4	0.884	0.051	2.16	0.13
p9@5	0.29	3.14	0.91	2.49	0.06	5.81	0.3	37.2	4.3	15.5	1.8	16.8	2.0	0.924	0.046	2.21	0.12
p5@1	1.06	2.97	0.78	4.61	0.05	11.13	2.7	36.3	8.1	15.4	3.4	19.4	4.3	0.792	0.073	1.87	0.18
p5@3	1.15	2.58	0.67	6.72	0.05	15.58	6.3	39.0	12.2	14.3	4.5	21.7	6.8	0.661	0.085	1.80	0.24
p5@4	1.19	1.77	0.73	3.11	0.05	7.42	6.6	36.6	5.5	14.4	2.1	19.8	2.9	0.730	0.045	1.85	0.12
p5@5	0.61	2.34	0.82	3.19	0.06	7.44	5.8	37.5	5.6	14.6	2.1	17.7	2.6	0.822	0.052	2.12	0.14
p5@6	0.88	2.43	0.76	4.22	0.06	9.75	2.8	33.6	6.6	13.8	2.7	17.8	3.5	0.773	0.065	1.89	0.17
p5@7	0.76	2.35	0.73	3.62	0.05	8.76	3.2	37.8	6.6	15.0	2.6	20.3	3.6	0.739	0.053	1.86	0.14
p8@2	0.73	2.02	0.82	2.67	0.06	6.10	3.5	32.9	4.0	13.9	1.7	17.0	2.1	0.817	0.044	1.93	0.11
p8@3	0.52	2.49	0.87	2.67	0.05	6.49	1.5	39.6	5.1	16.4	2.1	18.8	2.4	0.870	0.046	2.10	0.12
p8@4	0.81	1.60	0.83	2.63	0.05	6.30	7.9	37.5	4.7	15.5	1.9	18.6	2.3	0.833	0.044	2.01	0.11

differentiation event that resulted in a reservoir with a significantly higher μ -value than previously documented for Mars. Thus, the monzonitic clasts in NWA 7533 record the signature for a previously unknown geochemical reservoir. Most $^{208}\text{Pb}/^{204}\text{Pb}$ and $^{206}\text{Pb}/^{204}\text{Pb}$ compositions lie on a linear trend with the SNC meteorites, indicating a consistent Martian κ -value (Fig. 4). Utilizing a simplified thermal history of the monzonitic clasts with a formation age from the zircon upper intercept at 4.428 Ga, a final resetting age of the apatite at 1.35 Ga, and the Pb isotopic compo-

sitions in feldspars, the U-Pb differentiation history of the source of the monzonite can be modeled.

To successfully model the U-Th-Pb differentiation, radiogenic in-growth of Pb from the decay of U and Th must be discounted. To achieve that, U/Pb ratios were measured in each analytical spot directly following Pb isotopic analysis with the assumption that if the more radiogenic Pb compositions were a result of in-growth from U, $^{206}\text{Pb}/^{204}\text{Pb}$ would be positively correlated with U/Pb. However, the U/Pb ratios measured in plagioclase and K-feldspar are similar (<0.4), do not correlate with Pb isotopic ratios, and

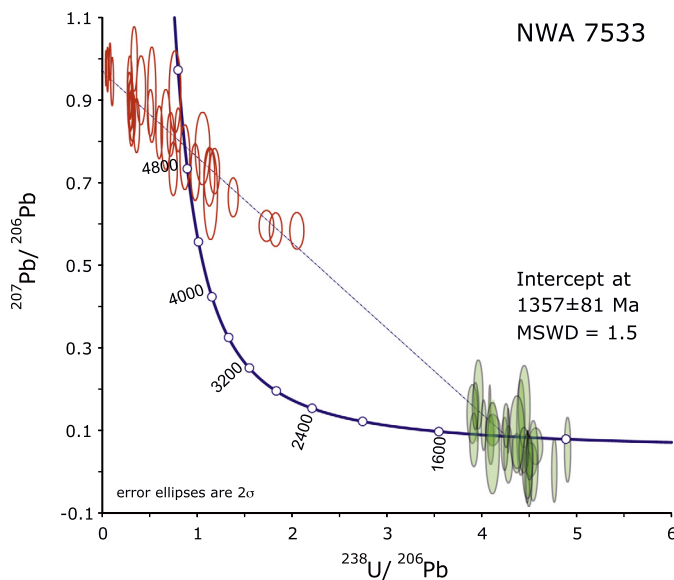


Fig. 2. Concordia-constrained linear 3-D isochron of phosphates in NWA 7533. Red ellipses represent actual data. Filled, green ellipses represent mathematical projections from actual data from the 3-D Concordia diagram onto a 2-D Tera-Wasserburg diagram. Calculated with Isoplot 3.75 (Ludwig, 2012). (For interpretation of the references to color in this figure legend, the reader is referred to the web version of this article.)

cannot account for the spread in isotopic data shown in Fig. 4, even after 4.4 Ga of U and Th decay (Table 1, Supplementary Fig. 2). As such, the more radiogenic data are interpreted as the result of resetting/mixing between feldspar and surrounding U-bearing minerals or micro-inclusions at 1.35 Ga.

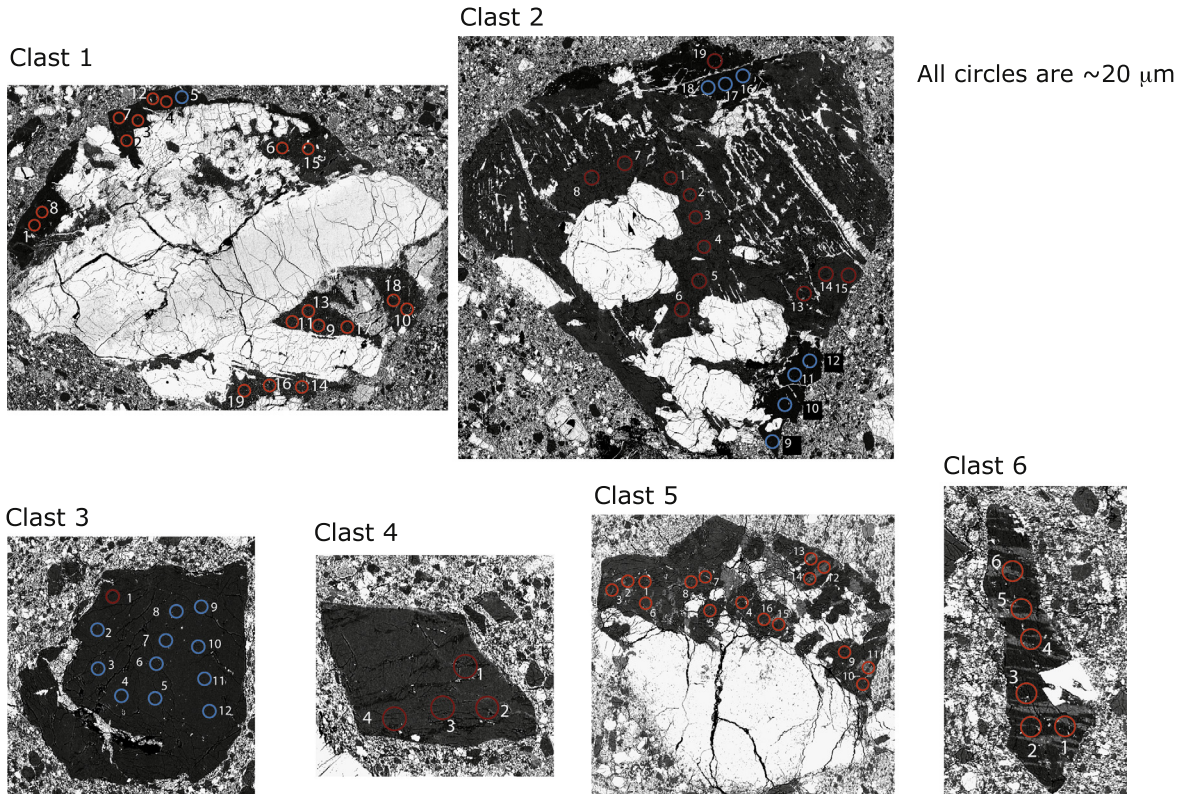


Fig. 3. Backscatter electron images and locations of spot analyses of all feldspar grains in clasts of NWA 7533. All circles are $\sim 20 \mu\text{m}$ in diameter. Blue circles represent non-radiogenic Pb (i.e., $^{206}\text{Pb}/^{204}\text{Pb} < 12$) and red circles represent radiogenic Pb (i.e., $^{206}\text{Pb}/^{204}\text{Pb} > 12$).

4.1. A single stage model of Pb evolution

Plagioclase is not particularly resistant to isotopic resetting in impact metamorphism but the least radiogenic plagioclase Pb population plots within error of the 4.428 Ga Geochron (Clasts 1, 2, and 3), which explicitly implies closed system U-Pb behavior in at least some of the feldspar grains. Therefore, single stage Pb growth μ -values can be calculated for the least radiogenic plagioclase data ($^{206}\text{Pb}/^{204}\text{Pb} < 11.5$, $n = 17$) by determining the intersection of a line with a slope equivalent to the age of the phosphates (1.35 Ga) through each of these data points and the 4.428 Ga Geochron. The weighted mean of these μ -values is 13.4 ± 1.7 (2σ). The overall uncertainty was determined by propagating the errors associated with the phosphate age and the errors associated with each Pb isotopic measurement (Supplementary Table 1, Fig. 5). This μ -value of 13.4 is ~ 3 times larger than that of any reservoir from which the SNCs were derived. These results imply one of two things: either 1) the Martian mantle is significantly more heterogeneous in μ -values than previously thought (i.e., having values between 1 and 14), or 2) the Martian crustal precursor to the monzonite was significantly more depleted in Pb or enriched in U than the source of the SNCs. Either hypothesis is indicative of a previously undocumented Martian geochemical reservoir formed prior to 4.43 Ga.

4.2. A two-stage model of Pb evolution

While a single stage Pb growth from 4.567 to 4.428 Ga with a μ -value of 13.4 can, in principle, explain the observed Pb isotopic data, it seems unlikely, especially since the precursor of the monzonite was Martian protocrust. Formation of this protocrust requires multiple episodes of differentiation and subsequent radiogenic Pb in-growth in the following reservoirs: 1) an undifferentiated, primitive reservoir before core formation, 2) a mantle

Table 2

Pb isotopic compositions and U/Pb of plagioclase and K-feldspar.

Analysis #	Feldspar type	$\frac{^{208}\text{Pb}}{^{204}\text{Pb}}$	2σ	$\frac{^{207}\text{Pb}}{^{204}\text{Pb}}$	2σ	$\frac{^{206}\text{Pb}}{^{204}\text{Pb}}$	2σ	$\frac{^{207}\text{Pb}}{^{206}\text{Pb}}$	2σ	$\frac{^{208}\text{Pb}}{^{206}\text{Pb}}$	2σ	U/Pb	2σ	
Clast 1*	(Clast K) 2-feldspars, zoned pigeonite, and augite													
1	Plagioclase	34.16	0.47	14.25	0.20	14.63	0.20	0.979	0.005	2.345	0.010	n.m		
2	Plagioclase	37.07	0.43	14.56	0.14	16.29	0.29	0.893	0.011	2.276	0.018	n.m		
3	Plagioclase	35.66	0.33	14.62	0.13	15.42	0.16	0.951	0.005	2.315	0.009	n.m		
4	Plagioclase	34.24	0.78	14.19	0.33	14.16	0.33	1.005	0.008	2.423	0.017	n.m		
5	Plagioclase	32.39	1.54	12.33	0.60	11.36	0.55	1.090	0.021	2.820	0.045	0.04	0.01	
6	K-feldspar	34.75	0.07	14.33	0.03	14.66	0.04	0.976	0.001	2.365	0.002	0.08	0.03	
7	Plagioclase	34.86	0.62	14.70	0.27	14.73	0.27	0.995	0.006	2.365	0.013	0.12	0.05	
8	Plagioclase	35.18	0.49	14.52	0.20	14.76	0.22	0.982	0.005	2.376	0.010	0.03	0.02	
9	K-feldspar	35.20	0.22	14.60	0.09	14.90	0.10	0.980	0.002	2.351	0.004	0.01	0.00	
10	K-feldspar	34.80	0.31	14.59	0.14	14.92	0.14	0.976	0.004	2.324	0.007	0.03	0.00	
11	K-feldspar	35.04	0.27	14.71	0.11	14.96	0.12	0.981	0.003	2.341	0.005	0.18	0.02	
12	Plagioclase	35.34	0.76	14.84	0.32	14.98	0.32	0.984	0.007	2.341	0.015	0.12	0.04	
13	K-feldspar	36.50	0.29	14.60	0.12	15.08	0.12	0.968	0.003	2.417	0.007	0.06	0.03	
14	K-feldspar	36.02	0.27	14.70	0.10	15.14	0.11	0.973	0.003	2.370	0.006	0.00	0.00	
15	K-feldspar	35.47	0.18	14.47	0.08	15.20	0.08	0.953	0.002	2.331	0.004	0.04	0.02	
16	K-feldspar	35.96	0.23	14.66	0.10	15.21	0.12	0.964	0.004	2.357	0.007	0.01	0.00	
17	K-feldspar	36.10	0.30	14.67	0.12	15.38	0.13	0.952	0.003	2.346	0.007	0.10	0.04	
18	K-feldspar	36.82	0.42	14.74	0.12	15.71	0.21	0.941	0.009	2.340	0.009	0.01	0.00	
19	K-feldspar	38.77	0.44	14.91	0.12	15.75	0.13	0.944	0.005	2.444	0.011	0.01	0.00	
Clast 2*	2-feldspars, augite, zircon 4 and zircon 12													
1	K-feldspar	34.85	0.44	14.64	0.19	14.89	0.19	0.980	0.004	2.332	0.009	0.04	0.03	
2	K-feldspar	34.63	0.55	14.60	0.24	14.86	0.24	0.979	0.006	2.321	0.011	0.00	0.00	
3	K-feldspar	35.10	0.49	14.76	0.21	15.20	0.21	0.976	0.005	2.311	0.010	0.01	0.01	
4	K-feldspar	35.04	0.34	14.77	0.15	15.15	0.15	0.975	0.004	2.304	0.008	0.08	0.05	
5	K-feldspar	35.05	0.47	14.65	0.18	15.10	0.22	0.976	0.005	2.329	0.009	0.01	0.00	
6	K-feldspar	35.12	0.39	14.76	0.16	15.07	0.17	0.981	0.004	2.323	0.008	0.01	0.00	
7	K-feldspar	34.87	0.29	14.69	0.13	15.00	0.13	0.981	0.003	2.319	0.006	0.17	0.06	
8	K-feldspar	34.80	0.36	14.67	0.16	14.96	0.16	0.982	0.004	2.323	0.007	0.36	0.09	
9	Plagioclase	30.83	0.36	12.05	0.23	10.94	0.21	1.100	0.008	2.822	0.018	0.00	0.00	
10	Plagioclase	31.68	0.48	12.47	0.20	11.48	0.21	1.084	0.008	2.752	0.024	0.00	0.00	
11	Plagioclase	31.10	0.46	12.14	0.18	11.07	0.17	1.096	0.006	2.801	0.014	0.00	0.00	
12	Plagioclase	30.75	0.43	11.96	0.17	10.73	0.16	1.113	0.006	2.861	0.014	0.00	0.00	
13	K-feldspar	35.19	0.49	14.94	0.21	15.13	0.21	0.987	0.005	2.325	0.010	0.07	0.02	
14	K-feldspar	34.42	0.31	14.57	0.13	14.76	0.13	0.985	0.003	2.333	0.006	0.00	0.00	
15	K-feldspar	34.84	0.52	14.75	0.22	14.93	0.23	0.985	0.005	2.326	0.010	0.27	0.09	
16	Plagioclase	30.29	0.51	11.71	0.20	10.48	0.18	1.116	0.008	2.898	0.017	0.08	0.05	
17	Plagioclase	30.67	0.62	11.80	0.24	10.38	0.22	1.128	0.009	2.941	0.021	0.05	0.03	
18	Plagioclase	31.06	0.74	11.88	0.29	10.54	0.26	1.119	0.011	2.905	0.025	0.16	0.01	
19	Plagioclase	34.68	0.64	14.62	0.27	14.82	0.28	0.986	0.006	2.348	0.013	0.10	0.04	
Clast 3	Plagioclase													
1	Plagioclase	34.25	1.15	13.86	0.47	13.34	0.46	1.039	0.013	2.564	0.027	0.08	0.02	
2	Plagioclase	32.68	1.33	12.81	0.53	11.25	0.47	1.134	0.019	2.852	0.039	0.00	0.00	
3	Plagioclase	31.71	1.25	12.37	0.50	10.78	0.44	1.155	0.018	2.943	0.040	0.02	0.01	
4	Plagioclase	32.13	1.16	12.91	0.47	11.81	0.44	1.099	0.015	2.734	0.033	0.00	0.00	
5	Plagioclase	30.41	1.09	11.76	0.43	10.22	0.38	1.158	0.017	2.953	0.037	0.02	0.01	
6	Plagioclase	30.72	1.24	11.59	0.48	10.30	0.43	1.142	0.019	3.003	0.043	0.01	0.01	
7	Plagioclase	30.72	1.23	11.83	0.47	10.54	0.42	1.116	0.017	2.881	0.038	0.00	0.00	
8	Plagioclase	31.88	1.23	12.50	0.49	10.65	0.42	1.155	0.018	2.983	0.040	0.41	0.18	
9	Plagioclase	31.36	1.05	12.18	0.42	10.79	0.37	1.135	0.016	2.932	0.040	0.00	0.00	
10	Plagioclase	31.07	1.46	12.15	0.59	10.56	0.51	1.169	0.023	2.968	0.049	0.00	0.00	
11	Plagioclase	31.47	1.20	12.02	0.47	10.50	0.41	1.155	0.018	2.986	0.040	0.00	0.00	
Clast 4	Perthite													
1	Perthite	38.13	2.46	15.23	0.99	15.32	1.06	1.029	0.024	2.537	0.050	0.00	0.00	
2	Perthite	33.62	1.85	13.57	0.76	13.34	0.75	1.028	0.024	2.556	0.052	0.28	0.06	
3	Perthite	36.94	1.46	15.11	0.58	15.17	0.58	0.997	0.012	2.404	0.025	0.03	0.01	
4	Perthite	36.68	1.78	15.47	0.80	15.20	0.75	1.005	0.017	2.455	0.036	0.01	0.01	
Clast 5*	Albite antiperthite, augite, zircons 5 and 6													
1	Anti-perthite	36.46	1.48	15.26	0.62	15.33	0.62	0.992	0.013	2.365	0.026	0.02	0.01	
2	Anti-perthite	34.09	0.66	13.89	0.27	13.94	0.27	0.993	0.007	2.444	0.016	n.m		
3	Anti-perthite	36.54	0.56	14.85	0.21	15.54	0.25	0.966	0.006	2.357	0.012	n.m		
4	Anti-perthite	34.85	0.59	14.25	0.24	14.46	0.26	0.993	0.007	2.395	0.012	n.m		
5	Anti-perthite	35.38	0.41	14.89	0.18	15.21	0.18	0.974	0.004	2.325	0.008	n.m		
6	Anti-perthite	33.61	0.63	13.64	0.26	13.55	0.26	1.007	0.007	2.478	0.014	n.m		
7	Anti-perthite	31.17	0.57	12.22	0.23	11.73	0.22	1.044	0.007	2.659	0.016	n.m		
8	Anti-perthite	35.53	0.49	14.51	0.20	15.41	0.22	0.945	0.005	2.304	0.009	n.m		
9	Anti-perthite	36.50	0.46	14.63	0.18	15.15	0.20	0.971	0.004	2.416	0.013	n.m		
10	Anti-perthite	35.47	0.44	14.76	0.19	15.09	0.19	0.976	0.004	2.349	0.009	n.m		
11	Anti-perthite	34.69	0.51	14.48	0.22	14.79	0.22	0.975	0.005	2.339	0.011	n.m		
12	Anti-perthite	35.31	0.26	14.38	0.11	14.90	0.11	0.966	0.003	2.369	0.005	n.m		
13	Anti-perthite	35.10	0.46	14.47	0.19	15.32	0.20	0.945	0.004	2.290	0.009	n.m		
14	Anti-perthite	34.95	0.40	14.46	0.17	14.87	0.17	0.972	0.004	2.342	0.008	n.m		
15	Anti-perthite	34.88	0.57	14.61	0.24	14.90	0.25	0.979	0.006	2.341	0.011	n.m		
16	Anti-perthite	33.87	0.64	14.01	0.27	13.98	0.27	1.002	0.007	2.423	0.014	n.m		
Clast 6*	Antiperthite with zircon 2													
6	1	Anti-perthite	34.86	0.84	14.63	0.36	15.08	0.37	0.962	0.009	2.304	0.016	n.m	
6	2	Anti-perthite	36.12	0.89	14.73	0.37	15.22	0.38	0.964	0.008	2.369	0.017	n.m	
6	3	Anti-perthite	34.63	0.77	14.57	0.34	15.01	0.34	0.972	0.008	2.311	0.016	n.m	
6	4	Anti-perthite	35.37	0.59	14.88	0.25	15.22	0.26	0.971	0.006	2.303	0.011	n.m	
6	5	Anti-perthite	34.31	0.74	14.29	0.31	14.96	0.33	0.951	0.008	2.287	0.016	n.m	
6	6	Anti-perthite	34.49	0.54	14.43	0.24	14.84	0.24	0.970	0.005	2.320	0.012	n.m	

* Mineralogical descriptions, specific details, and U-Pb in zircon for these clasts can be found in Humayun et al. (2013).

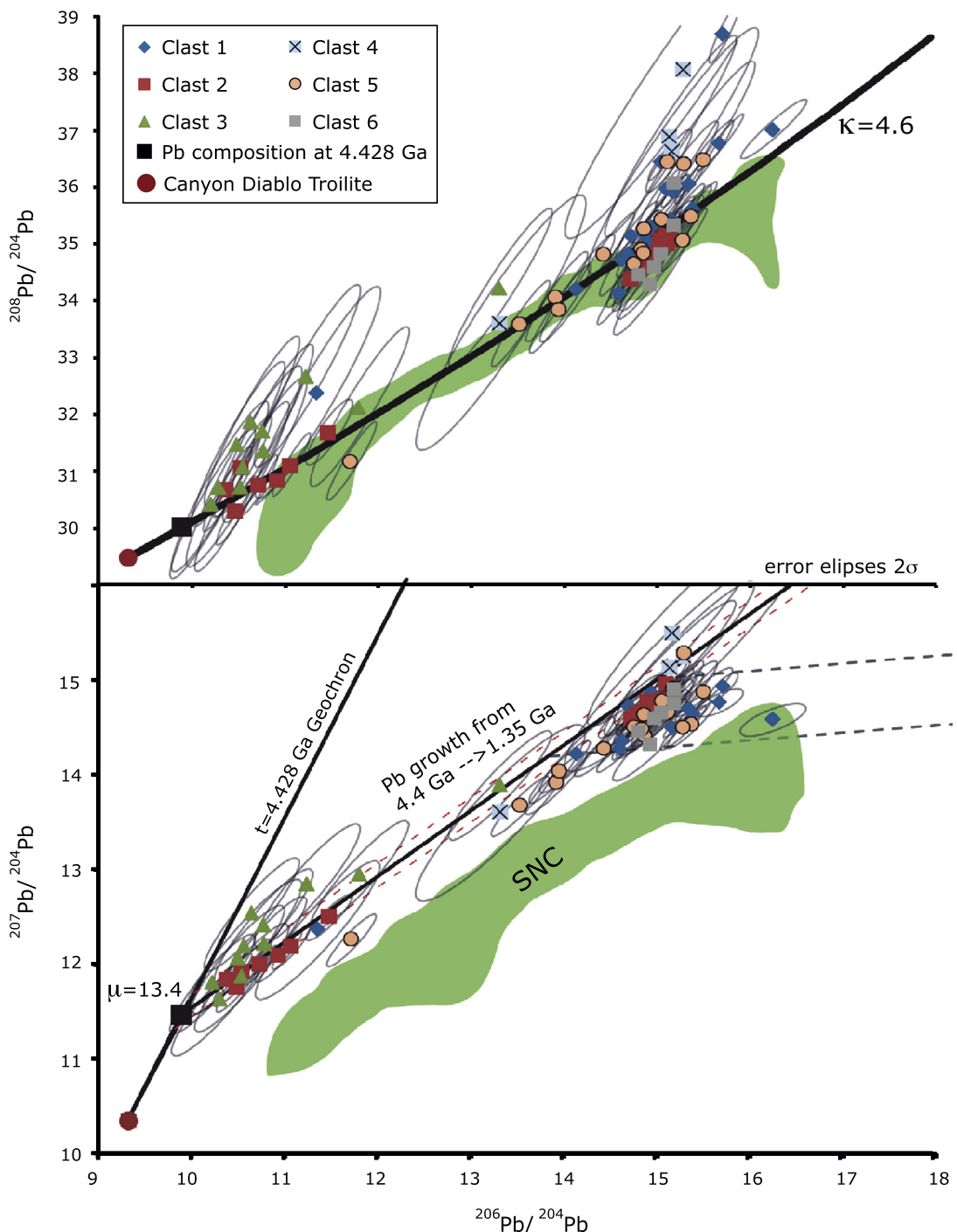


Fig. 4. Pb isotopic compositions of feldspar measured in monzonitic and matrix-bound clasts in NWA 7533. The green field represents Pb isotopic compositions of leached Martian meteorites and mineral separates (Borg et al., 2005; Bouvier et al., 2005, 2008, 2009; Gaffney et al., 2007). Pb growth line represents all Pb isotopic compositions from 4.428 Ga to 1.35 Ga originating with an initial Pb isotopic composition indicated by the black square. This composition is a result of Pb growth from 4.567 Ga to 4.428 Ga with a μ -value of 13.4, with red lines indicating 2σ error. Dotted grey lines represent Pb growth from 1.35 Ga to present indicating that some of the reset feldspars might contain small amounts of U, were reset recently (perhaps during impact), or display open system behavior. (For interpretation of the references to color in this figure legend, the reader is referred to the web version of this article.)

after the core was extracted, 3) various Martian mantle silicate reservoirs (i.e., the source of depleted, intermediate, and enriched shergottites, e.g., Debaillé et al., 2007), and 4) protocrust. Mars may have accreted rapidly (Dauphas and Pourmand, 2011), therefore, Pb growth in a primitive reservoir had to have been limited. Age constraints for the Martian core range from 1–15 Ma after CAI formation (Dauphas and Pourmand, 2011; Foley et al., 2005; Kleine et al., 2004; Nimmo and Kleine, 2007). Silicate differentiation resulting in the SNC reservoirs is proposed to have happened

~20–60 Ma after CAIs (e.g., Debaillé et al., 2007; Foley et al., 2005; Kleine et al., 2004). Silicate-only fractionation has a minor effect on U/Pb (e.g., Borg et al., 2005 and Gaffney et al., 2007). Therefore, metal separation (during core formation) or precipitation of sulfides is needed to create a high- μ reservoir. Sulfides will incorporate Pb but not U, increasing μ but not κ , precisely as observed in the data presented. Therefore, the two largest fractionation events to produce the necessary reservoir took place in either the mantle or the crust. The SNC mantle reservoir has a μ -value of 1–5,

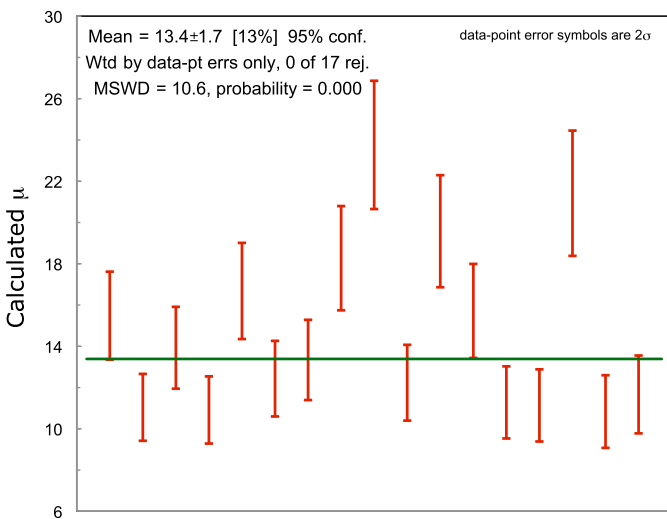


Fig. 5. Weighted average, order determined by increasing $^{206}\text{Pb}/^{204}\text{Pb}$ from lowest to highest from left to right for the calculated initial (4.567 Ga–4.428 Ga) μ -values.

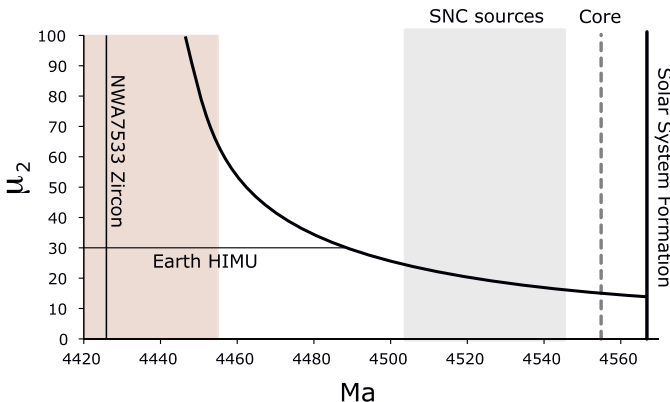


Fig. 6. A two-stage model of differentiation with time of differentiation vs. modeled μ_2 . μ_2 represents the μ -value needed to reach the initial Pb isotopic composition at 4.428 Ga, at any time since solar system formation if the protocrust was extracted from an SNC-like mantle with a μ -value of 3. Red field indicates error on zircon age determination from Humayun et al. (2013). Data for SNC source formation and core segregation from Foley et al. (2005).

so there is a possibility that the sources of the monzonite resided in an unusual mantle region that could have formed by more extreme removal of sulfides during core-formation, a source that is not sampled by any other lithology analyzed to date.

Alternatively, the high- μ source of monzonite formed by secondary differentiation of a protocrust derived from the primitive mantle. In this case, it is likely that the increase in μ occurred during partial silicate melting, perhaps in large impact melt sheets, with subsequent precipitation of sulfides. Additionally, Pb is a volatile element and a large volatilization event (i.e., large impact) or a series of volatilization and/or sulfide precipitation events closely spaced in time would have a similar influence on μ and κ .

If we assume that Martian core formation left a relatively homogeneous chemical signature on the Martian mantle and that the protocrust was derived from a Martian mantle that is SNC-like (average μ of 3, range ~1–5), the second stage, radiogenic crustal μ can be modeled based on the time of crustal differentiation (Fig. 6). The curve in Fig. 6 is representative of the μ -value necessary to reach the initial Pb isotopic composition in Fig. 4 at 4.428 Ga (black square), assuming a 2-stage growth with an initial, SNC-like μ -value of 3. This is a gross over-simplification of the Pb history of the monzonite, as stated above, but seems reasonable considering core formation and crustal differentiation involving

sulfides likely had the largest effects on μ . If the high- μ reservoir formed contemporaneously with the SNC reservoirs, the μ_2 value increases and approaches the μ -value for the HIMU reservoir on Earth (e.g., Nebel et al., 2013, Fig. 6). Regardless of the mechanism of μ increase, whether it be in the mantle, in the crust, or a combination of both, it must have happened prior to 4.428 Ga. Interestingly, the isotopic signature of a similar high μ -reservoir signature has been observed in Eoarchean (3.8 Ga) rocks on Earth, also requiring early U/Pb differentiation (ca. 4.1–4.3 Ga) and long-term reservoir isolation (Kamber et al., 2003).

5. Conclusions

The Pb isotopic compositions of plagioclase and K-feldspar in monzonitic clasts and matrix-bound feldspar in NWA 7533 record the signature of a previously unrecognized early geochemical reservoir on Mars that had a μ -value of at least 13.4. This μ -value is significantly higher than that of the reservoir sampled by the SNC meteorites. This high- μ reservoir likely represents the first isotopic evidence for a differentiated crust on Mars, in addition to the already documented depleted, intermediate, and enriched mantle reservoirs represented by the SNCs. Given that the bulk composition of NWA 7533 is closer in composition to the rocks and soils observed on the Martian surface than the SNCs, it may provide a more representative (and radiogenic) sample to study the differentiation history of the Martian crust than the SNC meteorites.

Acknowledgements

This work was funded by grants from the Knut and Alice Wallenberg Foundation (2012.0097) and the Swedish Research Council (VR 621-2012-4370) to MJW and AAN, and NASA NNX13AI06G to MH. The authors would like thank five anonymous reviewers for their insightful comments that greatly improved this manuscript. The Nordsim ion microprobe facility operates as a Nordic infrastructure regulated by The Joint Committee of the Nordic Research Councils for Natural Sciences (NOS-N). This is Nordsim publication #386.

Appendix A. Supplementary material

Supplementary material related to this article can be found online at <http://dx.doi.org/10.1016/j.epsl.2014.11.018>.

References

- Agee, C.B., Wilson, N.V., McCubbin, F.M., Ziegler, K., Polyak, V.J., Sharp, Z.D., Asmerom, Y., Nunn, M.H., Shaheen, R., Thiemens, M.H., Steel, A., Fogel, M.L., Bowden, R., Glamoclija, M., Zhang, Z., Elardo, S.M., 2013. Unique meteorite from Early Amazonian Mars: water-rich basaltic breccia Northwest Africa 7034. *Science* 339, 780–785.
- Asmerom, Y., Jacobsen, S.B., 1993. The Pb isotopic evolution of the Earth: inferences from river water suspended loads. *Earth Planet. Sci. Lett.* 115, 245–256.
- Borg, L.E., Edmunson, J.E., Asmerom, Y., 2005. Constraints on the U-Pb isotopic systematics of Mars inferred from a combined U-Pb, Rb-Sr, and Sm-Nd isotopic study of the Martian meteorite Zagami. *Geochim. Cosmochim. Acta* 69, 5819–5830.
- Bouvier, A., Blöcher-Toft, J., Vervoort, J.D., Albarède, F., 2005. The age of SNC meteorites and the antiquity of the Martian surface. *Earth Planet. Sci. Lett.* 240, 221–233.
- Bouvier, A., Blöcher-Toft, J., Vervoort, J.D., Gillet, P., Albarède, F., 2008. The case for old basaltic shergottites. *Earth Planet. Sci. Lett.* 266, 105–124.
- Bouvier, A., Blöcher-Toft, Janne, Albarède, F., 2009. Martian meteorite chronology and the evolution of the interior of Mars. *Earth Planet. Sci. Lett.* 280, 285–295.
- Boynton, W.V., Taylor, G.J., Evans, L.G., Reedy, R.C., Starr, R., Janes, D.M., Kerry, K.E., Drake, D.M., Kim, K.J., Williams, R.M.S., Crombie, M.K., Dohm, J.M., Baker, V., Metzger, A.E., Karunatillake, S., Keller, J.M., Newsom, H.E., Arnold, J.R., Brückner, J., Englert, P.A.J., Gasnault, O., Sprague, A.L., Mitrofanov, I., Squyres, S.W., Trombka, J.I., d'Uston, L., Wänke, H., Hamara, D.K., 2007. Concentration of H, Si, Cl, K, Fe, and Th in the low- and mid-latitude regions of Mars. *J. Geophys. Res., Planets* 112, E12S99.

- Chen, J.H., Wasserburg, G.J., 1983. The isotopic composition of silver and lead in 2 iron-meteorites—Cape-York and Grant. *Geochim. Cosmochim. Acta* 47, 1725–1737.
- Chen, J.H., Wasserburg, G.J., 1986. Formation ages and evolution of Shergotty and its parent planet from U-Th-Pb systematics. *Geochim. Cosmochim. Acta* 50, 955–968.
- Cherniak, D.J., Lanford, W.A., Ryerson, F.J., 1991. Lead diffusion in apatite and zircon using ion-implantation and Rutherford backscattering techniques. *Geochim. Cosmochim. Acta* 55 (6), 1663–1673.
- Chamberlain, K.R., Bowring, S.A., 2001. Apatite–feldspar U–Pb thermochronometer: a reliable, mid-range (450 °C), diffusion-controlled system. *Chem. Geol.* 172, 173–200.
- Clark, B.C., Baird, A.K., Weldon, R.J., Tsusaki, D.M., Schabel, L., Candelaria, M.P., 1982. Chemical composition of Martian fines. *J. Geophys. Res.* 87, 10059–10067.
- Dauphas, N., Pourmand, A., 2011. Hf–W–Th evidence for rapid growth of Mars and its status as a planetary embryo. *Nature* 473, 489–493.
- Debaille, V., Brandon, A.D., Yin, Q.-Z., Jacobsen, B., 2007. Coupled ^{142}Nd – ^{143}Nd evidence for a protracted magma ocean in Mars. *Nature* 450, 525–528.
- Foley, C.N., Economou, T., Clayton, R.N., 2003. Final chemical results from the Mars Pathfinder alpha proton X-ray spectrometer. *J. Geophys. Res.* 108, 8096.
- Foley, C.N., Wadhwa, M., Borg, L.E., Janney, P.E., Hines, R., Grove, T.L., 2005. The early differentiation history of Mars from ^{182}W – ^{142}Nd isotope systematics in the SNC meteorites. *Geochim. Cosmochim. Acta* 69, 4557–4571.
- Gaffney, A.M., Borg, L.E., Connelly, J., 2007. Uranium–lead isotope systematics of Mars inferred from the basaltic shergottite QUE 94201. *Geochim. Cosmochim. Acta* 71, 5016–5031.
- Gancarz, A., Wasserburg, G., 1977. Initial Pb of the Amitsqoq gneiss, West Greenland, and implications for the age of the Earth. *Geochim. Cosmochim. Acta* 41 (9), 1283–1301.
- Gellert, R., Rider, R., Brückner, J., Clark, B.C., Dreibus, G., Klingelhöfer, G., Lugmair, G., Ming, D.W., Wänke, H., Yen, A., Zipfel, J., Squyres, S.W., 2006. Alpha Particle X-Ray Spectrometer (APXS): results from Gusev crater and calibration report. *J. Geophys. Res.* 111, E02S05.
- Grange, M.L., Nemchin, A.A., Pidgeon, R.T., Timms, N., Muhling, J.R., Kennedy, A.K., 2009. Thermal history recorded by the Apollo 17 impact melt breccia 73217. *Geochim. Cosmochim. Acta* 73, 3093–3107.
- Grieve, Richard A.F., Stoeffler, Dieter, Deutsch, Alex, 1991. The Sudbury structure – controversial or misunderstood? *J. Geophys. Res.* 96, 22,753–22,764.
- Holmes, A., 1946. An estimate of the age of the Earth. *Nature* 157, 680–684.
- Houtermans, F., 1946. Die Isotopenhäufigkeiten im natürlichen Blei und das Alter der Urans. *Naturwissenschaften* 33, 185–286.
- Humayun, M., Nemchin, A., Zanda, B., Hewins, R.H., Grange, M., Kennedy, A., Loland, J.-P., Göpel, C., Fieni, C., Pont, S., Deldicque, D., 2013. Origin and age of the earliest Martian crust from meteorite NWA 7533. *Nature* 503, 513–517.
- Kamber, B., Collerson, K., Moorbat, S., Whitehouse, M., 2003. Inheritance of early Archaean Pb-isotope variability from long-lived Hadean protocrust. *Contrib. Mineral. Petro.* 145 (1), 25–46.
- Kleine, T., Mezger, K., Münker, C., Palme, H., Bischoff, A., 2004. ^{182}Hf – ^{182}W isotope systematics of chondrites, eucrites, and martian meteorites: chronology of core formation and early mantle differentiation in Vesta and Mars. *Geochim. Cosmochim. Acta* 68, 2935–2946.
- Lee, D.C., Halliday, A.N., 1995. Hafnium–tungsten chronometry and the timing of terrestrial core formation. *Nature* 388, 854–857.
- Levchenkov, O.A., Shukolyukov, Yu.A., 1970. A new method for calculating age and time of metamorphism of minerals and rocks without correction for ordinary lead. *Geochem. Int.* 1, 60–65.
- Ludwig, K.R., Silver, L.T., 1977. Lead-isotope inhomogeneity in Precambrian igneous K-feldspars. *Geochim. Cosmochim. Acta* 41 (10), 1457–1471.
- Ludwig, K.R., 2012. User's manual for Isoplot3.75: a geochronological toolkit for Microsoft Excel. Spec. Publ., No. 5. Berkeley Geochronological Center.
- McSween, H.Y., Taylor, G.J., Wyatt, M.B., 2009. Elemental composition of the Martian crust. *Science* 324, 736–739.
- Nakamura, N., Unruh, D.M., Tatsumoto, M., Hutchison, R., 1982. Origin and evolution of the Nakhlite meteorite inferred from the Sm–Nd and U–Pb systematics and REE, Ba, Sr, Rb abundances. *Geochim. Cosmochim. Acta* 46, 1555–1573.
- Nebel, O., Arculus, R.J., van Westrenen, W., Woodhead, J.D., Jenner, F.E., Nebel-Jacobsen, Y.J., Wille, M., Eggins, S.M., 2013. Coupled Hf–Nd–Pb isotope covariations of HIMU oceanic island basalts from Mangaia, Cook–Austral islands, suggest an Archean source component in the mantle transition zone. *Geochim. Cosmochim. Acta* 112, 87–101.
- Nemchin, A.A., Pidgeon, R.T., Healy, D., Grange, M.L., Whitehouse, M.J., Vaughan, J., 2009. The comparative behaviour of apatite–zircon U–Pb systems in Apollo 14 breccias: implications for the thermal history of the Fra Mauro Formation. *Meteorit. Planet. Sci.* 44 (11), 1717–1734.
- Nemchin, A.A., Whitehouse, M.J., Grange, M.L., Muhling, J.R., 2011. On the elusive isotopic composition of lunar Pb. *Geochim. Cosmochim. Acta* 75, 2940–2964.
- Nimmo, F., Kleine, T., 2007. How rapidly did Mars accrete? Uncertainties in the Hf–W timing of core formation. *Icarus* 191, 497–504.
- Nyquist, L.E., Bogard, D.D., Shih, C., Greshake, A., Stöffler, D., Eugster, O., 2001. Ages and geologic histories of Martian meteorites. *Space Sci. Rev.* 96, 105–164.
- Oversby, V., 1978. Lead isotope systematics of Archean plutonic rocks. *Earth Planet. Sci. Lett.* 38 (1), 237–248.
- Rose-Koga, E.F., Koga, K.T., Schiano, P., LeVoyer, M., Shimizu, N., Whitehouse, M.J., Clocchiatti, R., 2012. Mantle source heterogeneity for South Tyrrhenian magmas revealed by Pb isotopes and halogen contents of olivine-hosted melt inclusions. *Chem. Geol.* 334, 266–279.
- Whitehouse, M.J., Kamber, B.S., Moorbat, S., 1999. Age significance of U–Th–Pb zircon data from early Archaean rocks of west Greenland—a reassessment based on combined ion-microprobe and imaging studies. *Chem. Geol.* 160 (3), 201–224.
- Whitehouse, M.J., Kamber, B.S., Fedo, C.M., Lepland, A., 2005. Integrated Pb- and S-isotope investigation of sulphide minerals from the early Archean of southwest Greenland. *Chem. Geol.* 222, 112–131.
- Woodhead, J.D., Hergt, J.M., 2000. Pb-isotope analyses of USGS reference materials. *Geostand. Geoanal. Res.* 24, 33–38.
- Yin, Q.-Z., McCubbin, F.M., Zhou, Q., Santos, A.R., Tartese, R., Li, X., Li, Q., Liu, Y., Tang, J., Boyce, J.W., Lin, Y., Yang, W., Zhang, J., Hao, J., Elardo, S.M., Shearer, C.K., Rowland, D.J., Lerche, M., Agee, C.B., 2014. An Earth-like beginning for ancient Mars indicated by alkali-rich volcanism at 4.4 Ga. In: Lunar and Planetary Science Conference. Abstract #1320.
- Zartman, R.E., Haines, S.M., 1988. The plumbotectonic model for Pb isotopic systematics among major terrestrial reservoirs—a case for bi-directional transport. *Geochim. Cosmochim. Acta* 52, 1327–1339.